ELSEVIER

Desalination 114 (1997) 253–275

DESALINATION

Analysis of single-effect evaporator desalination systems combined with vapor compression heat pumps

Faisal Al-Juwayhel*, Hisham El-Dessouky, Hisham Ettouney

Chemical Engineering Department, Kuwait University, PO Box 5969, Safat 13060, Kuwait
Fax: +965 483-9498; E-mail: fjuwayhel@kucol.kuniv.edu.kw

Received 25 August 1997; accepted 8 October 1997

Abstract

A comparison was performed for four different types of single-effect evaporator desalination systems. The systems are driven by vapor compression heat pumps including thermal (TVC), mechanical (MVC), absorption (ABVC), and adsorption (ADVC). The study includes the development of mathematical models for the four systems. The models include equations for energy and mass conservation. In addition, design equations are used to determine the heat transfer areas in the evaporator and the condenser. The analysis is based on comparison of the performance ratio, specific power consumption, specific heat transfer area, and specific cooling water flow rate. For the four systems the specific surface area for the evaporator and the condenser is decreased upon the increase of the boiling temperature. The performance ratio for the thermal vapor compression system is decreased as the boiling temperature and pressure of motive steam are increased. In the MVC system, the specific power consumption is found to decrease with the increase of the boiling temperature and its difference with the temperature of the compressed vapor. The ABVC and ADVC systems have higher potential than the other two configurations. This is because of the higher performance ratio found in both systems and the generation of hot utility water.

Keywords: Desalination processes; Vapor compression; Heat pumps; Thermal desalination; Vapor reheat

1. Introduction

During the past four decades, rapid progress has occurred in the technology, production volume, and market value of the water desalination industry. In 1960 the number of desalination plants included five production units with a total production rate of 5,000 m^3/d. The number in 1995 stands at 11,066 with a capacity of 20.3×10^6 m^3/d [1]. This capacity is expected to double within the next 20 years. Desalination is

*Corresponding author in the Department of Mechanical Engineering.

PII S0011-9164(98)00017-4

now in use for fresh water supply in 120 countries around the world, and its market value is $\$5\times10^9$/y.

Nevertheless, water shortages are found in many countries around the world. The majority of these countries do not have the means to meet the high capital and running costs of large desalination plants, which include multi-stage flash desalination (MSF), reverse osmosis (RO), or multiple effect evaporation (MEE). This problem is addressed to a large extent by the design and development of single-effect evaporator desalination processes. Such systems are planned with a strong emphasis on their production capacity and cost. A single-effect evaporator desalination unit must have sufficient production volume, low capital requirements, low operating costs, and simple operating and maintenance procedures. The development of such systems makes the desalination process more accessible to hard- pressed communities, arid regions, and countries with limited means. Single-effect systems are constructed with features such as compactness, simple chemical pretreatment, high thermal efficiency, high heat transfer coefficient, low pumping power, and high operating flexibility. The most common single-effect evaporator- desalination system is mechanical vapor compression (MVC). Other systems, which include thermal vapor compression (TVC) and hybrid systems with absorption and adsorption heat pumps, are in the stage of conceptual design and analysis [2,3].

The majority of operating desalination plants in the Middle East is the MSF system. Wade [4] performed an extensive economic analysis on the RO process and other thermal desalination processes which include MSF, MEE-TVC and MEE-MVC. A comparison was based on the performance ratio, energy consumption, and primary energy consumption. Wade [4] concluded that large thermal desalination plants are competitive with the RO process in regions with low energy costs, especially in the Gulf countries. Moreover, the RO process has low tolerance to difficult seawater conditions and severe operating conditions. However, the RO process might have the edge in regions with high energy cost. The author concluded that the MEE process has many attractive features to dominate in the near future the desalination market for plants with small to medium production rates.

Morin [5] reported similar findings in his technical and economical comparison of the low temperature MEE and the conventional MSF desalination process. The study showed that the MSF process needs about half as much heat transfer surface area required for the low temperature MEE process. The MEE process offers a recovery of almost 50% higher than the MSF process for equal performance ratio. This results in smaller brine circulating pumps, piping systems and pretreatment equipment. The electrical energy use for the pumping processes favors the MEE process over the MSF system by a factor of about 30% for the same performance ratio. The study showed a total production cost of $\$1.86/m^3$ for the MSF process and $\$1.49/m^3$ for the MEE system. These results were consistent with a previous study by Hess and Morin [6]. The study indicated that the water costs at the distribution point are (1997 basis): MEE, $\$1.35/m^3$ and RO, $\$1.058/m^3$.

The analysis presented by Darwish and El-Dessouky [7] predicts that the second generation in water desalination plants will be settled between RO and MEE. The MEE desalination system is more efficient, from a thermodynamic and heat-transfer point of view, than the predominant MSF desalination system. The pumping power and the specific heat transfer area required for the MEE system, in a respective way, are about 20% and 50% of that needed for the MSF plants. Moreover, instead of engineering and construction of 24 stages in the MSF plants, only 10 partitions are needed in MEE plants having the same performance as that of the MSF plant. This indicates that the capital cost of the MEE system is expected to be about 50% less than that of MSF distillation system.

Rautenbach [8] stated that substantially lower primary energy consumption could be achieved in thermal desalination processes by the MEE principle. Horizontal tube multiple-effect (HTME) units can be operated economically with very small driving force designed with a high gain ratio even for low top brine temperatures, and it is a superior process compared to the standard MSF process. However, Rautenbach et al. [9] pointed out that the MEE process has the potential of competing with MSF with respect to simplicity and with RO with respect to specific exergy (or primary energy) consumption. Although large units can be built, it remains an open question whether they will be ordered.

Modeling, simulation, and analysis of the MEE system are limited to a small number of literature studies. Most of the studies adopted many simplifying assumptions, which reduced the model capabilities in accurately predicting system parameters with a strong influence on the production cost [10–13]. These shortcomings were addressed recently by El-Dessouky et al. [14] upon development of a complete mathematical model for the MEE process. The model features negate the shortcomings found in the literature models. These features are as follows:

- The basic assumption in the model is the practice case of constant heat transfer areas for both the evaporators and feed heaters in all effects. This is necessary to improve the economy and the construction of the plant.
- It considered the effect of the vapor leak to the venting system.
- It contemplated the variation in the thermodynamic losses (boiling point elevation, non-equilibrium allowance inside the evaporators and the flashing boxes, temperature depression corresponding to the pressure drop in the demister, vapor transmission lines, and during the condensation process) from one effect to another.
- It studies the effect of boiling temperature, velocity of brine flowing through the tubes of feed heaters, the tube material of construction, and tube bundle geometry on the required specific heat transfer area.
- It takes into consideration the effect of water temperature and salinity on the water physical properties such as density, latent heat of evaporation, viscosity, Prandtl number and specific heat at constant pressure.
- It weights the effect of the presence of non-condensable gases on the heat transfer coefficients in the evaporators and the feed heaters.

Subsequent applications of the above model were made for the single-effect TVC [2] and the hybrid systems of MEE and various types of heat pumps [3]. El-Dessouky [2] found operation of the TVC system at higher steam temperatures reduces the specific heat transfer area, which lowers the system capital cost. Also, operation at high steam temperatures improves the system performance, which reduces the system energy consumption. In addition, system analysis shows reduction in the amount of the specific cooling water flow rate. This factor affects the initial cost, in terms of the size reduction of the down condenser and seawater feed pump, and the energy consumption rate, in terms of reducing the seawater pumping power. The study by El-Dessouky and Ettouney [3] investigated the possibilities of increasing the performance ratio by more than a factor of two in hybrid systems of MEE and various types of heat pumps. The following systems were considered in their analysis:

- MEE combined with thermal vapor compression (MEE-TVC)
- MEE combined with mechanical vapor compression (MEE-MVC)
- MEE combined with zeolite-water heat pump (MEE-ADS), and
- MEE combined with LiBr-water heat pump (MEE-ABS).

The results reported by El-Dessouky et al. [3] predict a large increase in the performance ratio of the hybrid systems. The increase varied from low values of 10–20% to higher values of close to 200%. These predictions are in line with existing MEE-TVC systems, which have a performance ratios close to 16 for units with 12 effects [15,16]. The analysis of the MEE-ADS and MEE-ABS show high system potential due its high performance ratio and possibility of combining with other valuable applications, i.e., district heating.

The original MEE-MVC systems were limited to operation of units with small capacities, less than $500\,m^3/d$, and high-energy consumption rates, $16\,kWh/m^3$. Success and reliability in operation of the small scale units have promoted development of medium- to large-scale units with capacities up to $3000\,m^3/d$ (0.8 mgd) and lower energy consumption, $6\,kWh/m^3$ [17–19]. A combination of MEE and mechanical vapor compression was motivated by the low capacity of the single-effect mechanical vapor compression. The combined MEE- MVC system has many advantages over conventional MSF or RO systems. These advantages include moderate investment cost, easy operation and maintenance, high reliability and long lifetime, inexpensive seawater pretreatment, and high purity distillate. In comparison with MSF, the MEE-MVC system is compact and requires less civil and construction work [20]. Comparison with the RO favors the MEE-MVC because of cost of feed pretreatment and operational reliability. Many of the advantages of the MEE-MVC are realized at low top brine temperatures (50–70°C) [20,21]. At low temperatures, problems caused by scaling and/or corrosion are absent or minimal. This increases the plant factor. However, most of the MVC plants operate in the single-effect mode.

Among the various seawater desalination processes of practical interest is the combined system of MEE and thermal vapor compression (MEE-TVC) system. The system has the following features: (1) its high performance ratio with fewer number of effects, (2) good flexibility to load variation, (3) simple geometry, and (4) absence of moving parts. The last feature makes the process robust, minimizes the required skill maintenance, and reduces the spare parts stocking. The process can be driven by superheated or saturated steam at low or intermediate pressures without formation of hot spots which augment scale formation. All these factors make the process a potential candidate for future application in large-scale installations. Michels [22] posed the following outstanding features of MEE with thermal vapor compression: low temperature operation lowering corrosion and scaling (top brine temperature is below 60°C), low energy consumption both thermal and electrical, short delivery time, easy operation and maintenance, and proven reliability in the Gulf region. Good economics in construction, civil work and seawater intake result in costs 35% less than for MSF plants.

Temstet and Laborie [15] outlined the main characteristic of a dual-purpose multi-effect desalination plant. The system is designed to switch automatically between two operating modes, which depends on the seasonal variations in power and water demand. The first mode combines the MEE system with a single-stage steam jet ejector, which compresses the vapor extracted from the last effect. The second mode of operation involves the use of low pressure heating steam. The plant operates over low temperature ranges includes 12 effects and has a production capacity of $12{,}000\,m^3/d$. A second system, which includes 12 effects and a steam-ejector vapor compression unit, is described by Temstet et al. [16]. The plant is comprised of four units, each producing $9{,}000\,m^3/d$ of distillate water. The steam ejectors are fed with 45-bar steam raised by dedicated boilers. The design gain output ratio (PR) of the units is 16.7.

Use of the LiBr-water absorption heat pump (MEE-ABS) or the zeolite-water adsorption heat pump is common in applications for air conditioning, heating, and ice making. An LiBr-water absorption heat pump is proposed by Alefeld and Ziegler [23] for water desalination. The system includes three stages, which process seawater and generates fresh water. Fathalah and Aly [24] analyzed a solar powered LiBr-water heat pump, which generates drive steam to an MEE system. More emphasis in their analysis was given to the performance of the solar power unit and air cooling in the evaporator unit. To the best of our knowledge, no previous attempts were made for analysis of the hybrid system of MEE and zeolite-water adsorption heat pump.

The main objective of this study is to present mathematical models of single-effect evaporator desalination units in hybrid systems with vapor compression heat pumps. The heat pumps include mechanical vapor compressor, thermal vapor compression, the LiBr-water absorption system, and the zeolite-water adsorption system. The analysis includes comparison of model results against actual data for the single-effect processes.

2. Analysis of single-effect evaporators

2.1. Thermal vapor compression

A schematic diagram for the single-effect thermal vapor compression (TVC) seawater desalination process is given in Fig. 1. The system constitutes an evaporator, a steam jet ejector, and a feed heater. The evaporator consists of an evaporator/condenser-heat exchanger, a vapor space, a water distribution system, and a mist eliminator. On the other hand, the steam jet ejector is composed of a steam nozzle, a suction chamber, a mixing nozzle, and a diffuser. The heater is a counter-current surface condenser in which the latent heat of the condensing vapor is transferred to the feed seawater.

A known mass of seawater is introduced into the tube side of the condenser. After being heated in the condenser, the seawater stream leaving the condenser is divided into two parts. The first and larger part, the cooling water, is rejected back to the sea and the second smaller part, the feed, is introduced into the evaporator. The function of the cooling water is the removal of the excess heat added to the system. This heat is added to the system in the form of motive steam, which drives

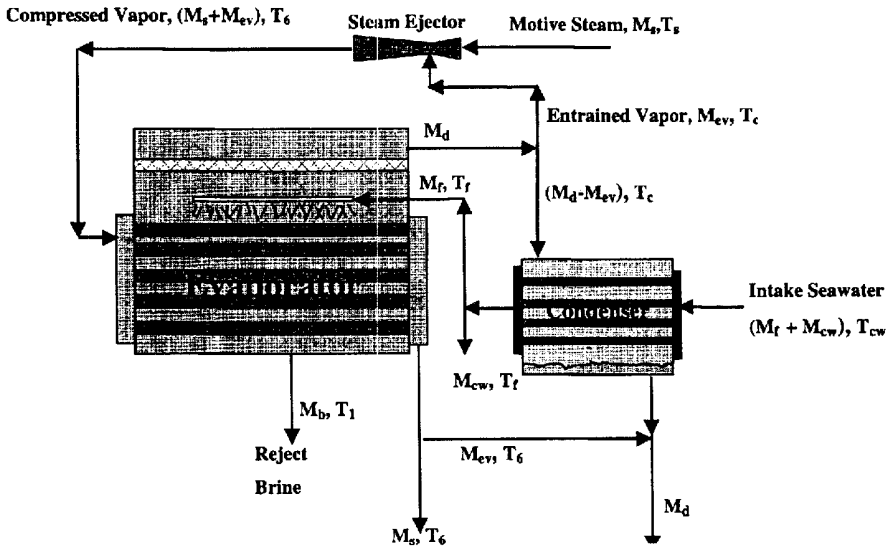

Fig. 1. Thermal vapor compression evaporator–desalination.

the steam jet ejector. It is important to emphasize here that the evaporator does not consume much of the supplied heat, it simply degrades it. The heating of the feed seawater in the condenser is essential to increase the thermal performance of the process. The heat source in the condenser is supplied by condensing a controlled portion of vapor formed by boiling in the evaporator. Accordingly, the condenser has three functions: (1) remove the extra heat from the system, (2) improve the process thermal efficiency, and (3) adjust the boiling temperature inside the evaporator.

Within the evaporator, the feed water is sprayed at the top where it falls in the form of thin film down the succeeding rows of tubes arranged horizontally. The feed water temperature is raised to the boiling temperature. The boiling temperature is dictated by the nature of chemicals used to control the scale formation and the state of the heating steam. This temperature is mastered through settling the pressure in the vapor space of the evaporator. The vapor formed by boiling is free of salts. The saturation temperature of the generated vapor is less than the boiling temperature by the boiling point elevation. The vapor flows through a knitted wire mist separator, demister, to remove the entrained brine droplets. The saturation temperature of the vapor departing the demister is reduced to lower value because of the frictional pressure loss in the demister. The vapor leaving the demister flows to the condenser where it splits into two parts. The first part condenses outside the tubes of the condenser and the steam jet ejector entrains the second part.

A schematic diagram for the steam jet ejector is given in Fig. 2. The diagram includes state points as well as the velocity and pressure profiles within the ejector. The ejector is used to increase the pressure of the entrained vapor. This process takes place through converting the pressure energy of the motive steam to generate vacuum and compress the entrained vapor to the required pressure. As the motive steam expands in the nozzle, its static pressure energy is converted to kinetic energy. The nozzle has a converging/diverging shape to expand the steam to velocities greater than the speed of sound (supersonic). The suction chamber is used to keep the nozzle properly positioned with respect to the diffuser and to direct the entrained vapor. The entrained vapor enters the suction chamber and mixes with the motive steam. The mixing process is violent and rapid. The two streams mix together as they pass through the converging section of the venturi diffuser. The mixture enters the throat section of the diffuser, completely mixed, at the sonic velocity of the mixture. The combined stream is self-compressed through the diverging section of the venturi diffuser where the cross sectional area increases and the velocity decreases, converting the kinetic energy of the mixture to static pressure energy. The mixture leaves the ejector at a pressure with an intermediate between that of the motive and the entrained vapor.

The mathematical model for the TVC system includes balance equations for the evaporator, condenser, and steam ejector. The model was developed after the study by El-Dessouky [7]. The total mass and the salt balance in the system are given by

$$M_f = M_d + M_b \tag{1}$$

$$M_b = M_d\left[X_f/\left(X_b - X_f\right)\right] \tag{2}$$

The evaporator thermal load, Q_e, is given by

$$Q_e = M_s\lambda_s = M_f C_p\left(T_b - T_f\right) + M_d\lambda_v \tag{3}$$

where C_p is the specific heat at constant pressure; M the mass flow rate; T the temperature; X the salt concentration; λ the latent heat; and the subscripts b, d, f, s, and v denote the brine, distillate, feed seawater, compressed vapor, and

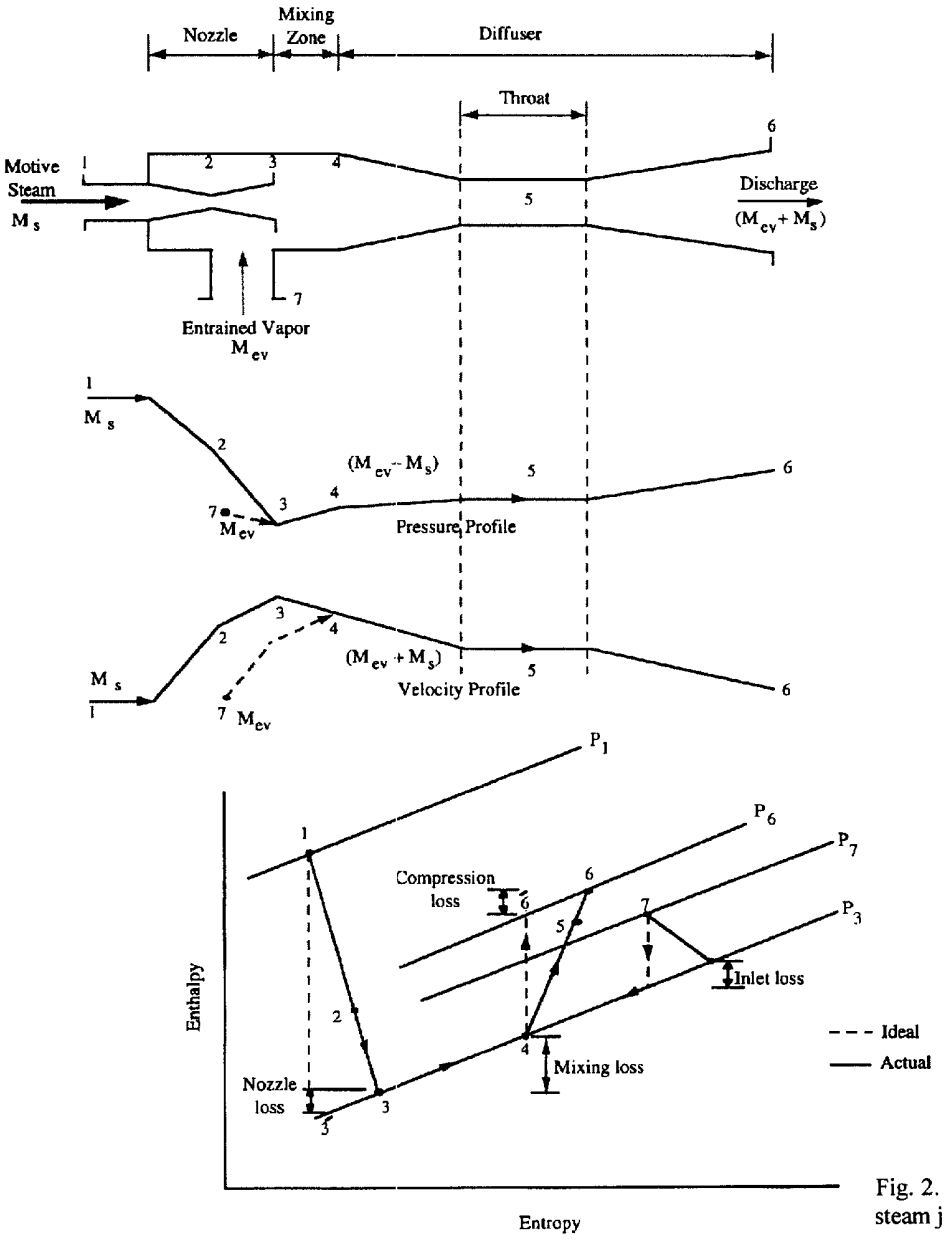

Fig. 2. Different processes in steam jet ejector.

vapor formed in the evaporator, respectively. The following relation is used to calculate the specific heat:

$$C_p = (A + BT + CT^2 + DT^3) \times 10^{-3} \quad (4)$$

with

$$A = 4206.8 - 6.6197S + 1.2288 \times 10^{-2} S^2$$

$$B = -1.1262 + 5.4178 \times 10^{-2} S - 2.2719 \times 10^{-4} S^2$$

$$C = 1.2026\times10^{-2} - 5.3566\times10^{-4}S + 1.8906\times10^{-6}S^2$$

$$D = 6.8777\times10^{-7} + 1.517\times10^{-6}S - 4.4268\times10^{-9}S^2$$

where T is the temperature in °C and S is the water salinity in gm/kg. The saturation temperature of the formed vapor is given by

$$T_b = T_v + BPE \tag{5}$$

The boiling point elevation (BPE), at a given pressure, is the increase in the boiling temperature due to the effect of dissolved salts. The value of the BPE is obtained from the following empirical formula

$$BPE = X(B + CX)10^{-3} \tag{6}$$

with

$$B = (6.71 + 6.34\times10^{-2}T + 9.74\times10^{-5}T^2)10^{-3}$$

$$C = (22.238 + 9.59\times10^{-3}T + 9.42\times10^{-5}T^2)10^{-8}$$

Eq. (6) is valid for the following ranges: $20{,}000 \le X \le 160{,}000$ ppm, $20 \le T \le 180$ °C. The required heat transfer surface area in the evaporator, A_e, is calculated from the following rate equation:

$$A_e = M_s\lambda_s / [U_e(T_s - T_b)] = [M_f C_p(T_b - T_f) + M_d\lambda_v]/[U_e(T_s - T_b)] \tag{7}$$

The overall heat transfer coefficient in the evaporator, U_e, is obtained from the correlation developed by El-Dessouky et al. [14]:

$$U_e = 1.9695 + 1.2057\times10^{-2}T_b - 8.5989\times10^{-5}T_b^2 + 2.565\times10^{-7}T_b^3 \tag{8}$$

where U_e is in kW/m^2°C and T_b in °C. Heat transfer between the condensing vapor and the feed seawater in the condenser can be written in terms of an overall heat transfer coefficient (U_c), condenser heat transfer area (A_c), and the logarithmic mean temperature difference $(LMTD)_c$; thus:

$$Q_c = U_c A_c (LMTD)_c \tag{9}$$

where $(LMTD)_c$ is defined by

$$(LMTD)_c = (T_f - T_{cw}) / \ln[(T_v - T_{cw})/(T_v - T_f)] \tag{10}$$

The thermal load of the condenser, Q_c, is given

$$Q_c = (M_{cw} + M_f) Cp(T_f - T_{cw}) = M_h\lambda_v \tag{11}$$

In the above equations T_{cw} is the feed seawater temperature, and M_h is mass flow rate of unentrained vapor. Combining Eqs. (9)–(11) produces

$$A_c = (M_{cw} + M_f) C_p \ln[(T_v - T_{cw})/(T_v - T_f)] / U_c \tag{12}$$

The overall heat transfer coefficient in the condenser is obtained from the correlation developed by El-Dessouky et al. [14]:

$$U_c = 1.7194 + 3.2063\times10^{-3}T_v + 1.5971\times10^{-5}T_v^2 - 1.9918\times10^{-7}T_v^3 \tag{13}$$

Design of the steam ejector is made by using the model previously developed by El-Dessouky [2]. The first equation in the model gives the compression ratio, Cr, of the compressed and the entrained vapors,

$$Cr = P_s / P_v \tag{14}$$

where P_s and P_v are the pressures of compressed and entrained vapor. The compression ratio can

be varied over a range from 1.8 to 5. Specification of its value together with the pressure of the entrained vapor is used to determine the pressure of the compressed vapor, which is assumed at saturation conditions. The entrainment ratio is defined as the mass flow rate of compressed vapor to the mass flow rate of entrained vapor. This ratio is obtained from the following relation:

$$Ra = 0.296\frac{(P_s)^{1.19}}{(P_v)^{1.04}}\left(\frac{P_m}{P_v}\right)^{0.015}\frac{(PCF)}{(TCF)} \quad (15)$$

$$PCF = 3\times10^{-7}(P_m)^2 - 0.0009(P_m) + 1.6101 \quad (16)$$

$$TCF = 2\times10^{-8}(T_v)^2 - 0.0006(T_v) - 1.0047 \quad (17)$$

where Ra is the entrainment ratio, which is defined as the mass of motive steam (M_m) per unit mass of entrained vapor (M_{ev}). P_m, P_s and P_v are the pressures of the motive steam, compressed vapor, and entrained vapor, respectively. PCF is the motive steam pressure correction factor and TCF is the entrained vapor temperature correction factor. The pressures, temperatures, and flow rates in the above equations are in kPa, °C, and kg/s, respectively. The above equation is valid in the following ranges: $Ra \leq 5$, $500 \geq T_m > 10$°C, $3500 \geq P_m \geq 100$ kPa, and $P_s/P_v \geq 1.81$.

To solve the above equation set it is necessary to specify the boiling temperature, the pressure of motive steam, the seawater temperature, and the compression ratio. Other specifications include the salt content in the feed and the rejected brine. The distillate flow rate is set at 1 kg/s, and the temperature of the feed seawater to the evaporator, T_f, is set at $(T_b - 5)$°C. Eqs. (1) and (2) are used to determine M_f and M_b. Eqs. (3), (7), and (8) are used to calculate the evaporator load, the heat transfer coefficient, and the heat transfer area. The ejector model [Eqs. (14)–(17)] is used to determine the entrainment ratio. Finally, Eqs. (9)–(13), together with the entrainment ratio, are used to calculate the condenser thermal load, heat transfer coefficient, and heat transfer area, as well as the flow rates of the cooling seawater, the entrained vapor, and the motive steam.

2.2 Mechanical vapor compression (MVC)

The MVC system is the most attractive among various single stage desalination processes. The MVC system is compact, confined, and does not require external heating source, which is opposite to the other three systems. The system is driven by electric power; therefore, it is suitable for small population areas with access to the power grid lines. Another advantage of the MVC system is the absence of the down condenser and the cooling water requirements. This is because the entire vapor formed in the last effect is routed to the compressor.

The disadvantages of the MVC system include:

- use of high quality electrical energy
- limitations imposed on the vapor compression range, which include flow rate of compressed vapor and temperature increase of the compressed vapor
- maintenance and spare parts requirements for the compressor moving parts, which include blades, shaft, sealing, and motor.

The first disadvantage limits the use of the MVC system in countries with limited energy resources, i.e., fossil, nuclear, or hydro. The second disadvantage limits the operation of the MVC system to low top brine temperatures, 60–70°C. This results in a larger heat transfer area for the evaporator unit, which increases the capital cost. In addition, the single unit production capacity is limited to 800 m^3/d (0.21 mgd). This problem is addressed to some extent by operating MVC and multi-effect evaporation units with 3 to 4 effects, where the capacity increases to 3,000 m^3/d (0.8 mgd) [17]. The last disadvantage increases

the operating cost and dictates use of highly skilled labor.

Energy conservation within the MVC system is maintained by recovery of energy in the rejected brine and the condensate steam. In addition, the temperature of the compressed vapor is raised to a higher level, which allows for vapor superheating. The superheating provides part of the thermal energy required for system operation. The analysis presented here focuses on system performance over a wide range for the boiling temperature. This is motivated by reduction in the areas of the evaporator and the heat exchange units at high boiling temperatures.

A schematic diagram for the proposed system is shown in Fig. 3. As is shown, the compressor operates on the vapor formed in the evaporator, where it is superheated to a temperature higher than the temperature of the boiling brine. The compressed vapor is introduced into the evaporator tubes; hence, it condenses after being cooled to its saturation temperature and releasing its latent heat. The condensate and the rejected brine have substantial amount of energy, which is recuperated in the feed heat exchanger. Therefore, the feed temperature is increased from a low value of 25°C to higher value within 3–6°C of the condensate and the rejected brine temperature.

The mathematical model of MVC includes mass balance, salt balance, and energy balances for the evaporator and heat exchangers. The mass and salt balance equations are identical to Eqs. (1) and (2), given in the TVC system. The evaporator and heat exchanger balances are given by

$$M_d\left[\lambda_s + C_{pv}\left(T'_s - T_s\right)\right] = M_d\lambda_v + M_f C_p\left(T_b - T_f\right) \tag{18}$$

$$M_f C_p\left(T_f - T_{cw}\right) = M_d C_p\left(T_s - T_o\right) + M_v C_p\left(T_b - T_o\right) \tag{19}$$

In Eqs. (17) and (18), it should be noted that the specific heat for different stream depends on the stream temperature and salinity. The latent heats λ_s and λ_v are calculated at the saturation temperatures T_s and T_v, respectively. The saturation temperature T_s is less than the compressed vapor temperature, T'_s, by the degree of superheating. Also, the formed vapor temperature, T_v, is lower than the brine boiling temperature, T_b, by the boiling point elevation. The effluent temperature for the rejected brine and condensed vapor from the heat exchangers is equal T_o.

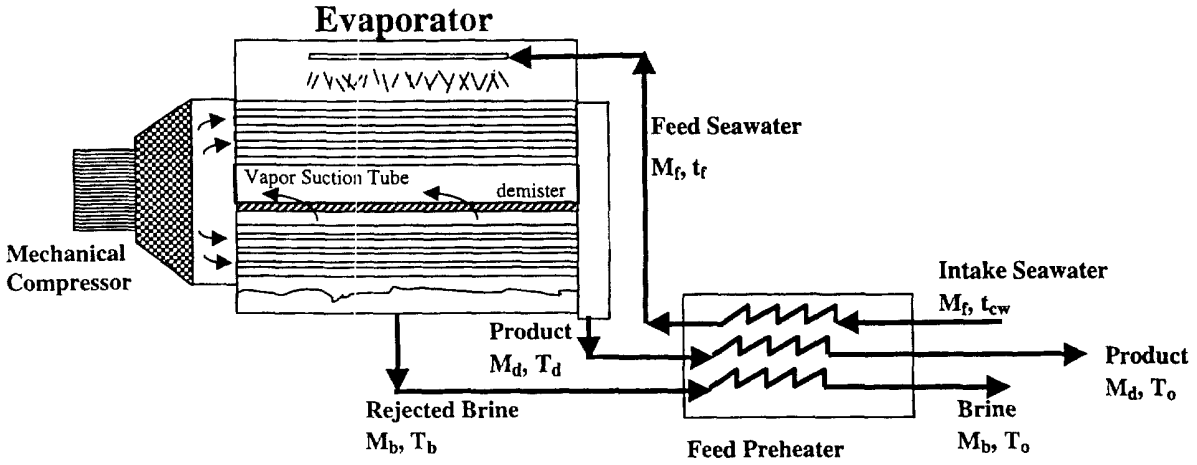

Fig. 3. Mechanical vapor compression evaporator-desalination process.

$$W = \gamma/[(\eta(\gamma-1)]P_v V_v\left[\left(P_s/P_v\right)^{[(\gamma-1)/\gamma]} - 1\right] \quad (20)$$

where W is the specific power consumption, kJ/m^3 vapor, P_v and P_s are the inlet and outlet pressures, kPa, V_v is the saturation specific volume of inlet vapor at T_v, η is the mechanical compressor efficiency, and γ is the isentropic compressibility factor. The vapor pressures, P_v and P_s, are calculated at the saturation temperature, T_v and T_s.

Solution of the above model requires specification of the temperatures of the boiling brine, T_b, the compressed vapor, T'_s and the condensing vapor, T_s. The evaporator balance is used to determine the feed temperature and the heat exchanger balance is used to determine the outlet temperature of the rejected brine and the condensed vapor. The flow rates in the system are obtained by solution of Eqs. (1) and (2). Finally, the workload of the compressor is calculated from Eq. (20).

2.3. Adsorption Vapor Compression (ADVC)

The adsorption-desorption heat pump is environmentally friendly. The pump uses benign fluids, which does not contribute to the destruction of the ozone layer. Its role in the greenhouse effect is negligible because the pump can be driven by renewable or waste energy sources and also to its high thermal efficiency. Moreover, the process is simple, does not include moving parts, has a long life, and is vibration free. For these reasons, in recent years, the adsorption-desorption heat pump has attracted increasing attention in the concern of replace the traditional compressor-based systems, which utilize ozone harmful fluids. Applications of the adsorption-desorption heat pumps are found in air-conditioning and in ice making. The ADVC system is shown diagrammatically in Fig. 4. The system includes the evaporator/condenser unit, two adsorption beds, and two heat exchangers. It is interesting to note that the evaporator and condenser form a single unit in this configuration, which replaces the individual condenser and evaporator in a conventional adsorption heat pump. Also, the liquid-to-liquid heat exchanger (HE2) preheats the feed seawater by condensed distillate product and reject brine. The adsorber (bed II in Fig. 4) plays the role of the bottom condenser in the TVC system. That is, this

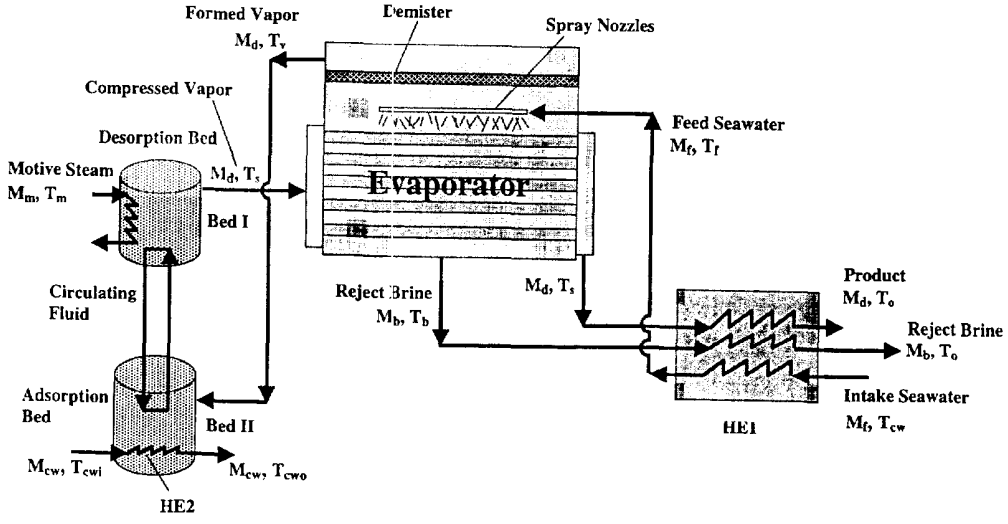

Fig. 4. Single-effect evaporator driven by an adsorption heat pump.

adsorber absorbs or rejects the excess heat added to the system in the second adsorber.

The closed cycle of the heat pump is composed of the following steps:

1. Initially, bed I is assumed to be cold and saturated with water. The mass of the bed is the mass of the adsorbent M_z plus the associated water M_{ev}. The temperature of the bed is T_a. The second bed is dry and hot at T_g. The temperature of the cold bed T_a must be less than the temperature of the water adsorbed in the bed. This temperature is fixed by the equilibrium relationship for the zeolite-water pair. On the other hand, the temperature of the hot bed T_g is equal to the temperature of heating steam flowing to the first effect. The first step commences when the circulating fluid starts to transfer heat between the two beds. Thus, heating the first bed and cooling the second bed occurs simultaneously. During this phase, no heat is exchanged between the adsorbers and any external heat source or sink. The heat flowing into the first adsorber, $Q_{2\text{-}1}$, is represented by the path abe_1 on the Clapeyron diagram, while the heat transferred from the second bed, $Q_{2\text{-}1}$, is described by the route cde_2 on the same diagram. The process is terminated when the first bed is heated to T_{e_1} and second bed is cooled to T_{e_2}. For the heat transfer to take place, T_{e_2} should be higher than T_{e_1}.

2. The second step starts when the first bed is connected to the external source of heating steam (boiler), where its temperature is increased from T_{e_2} to T_g. At the same time, a stream of cooling-water is used to reduce the second bed temperature from T_{e_2} to T_a.

3. During the heating process and once the pressure inside the first bed becomes higher than the condenser pressure, the bed is opened to the tube side the of the evaporator where the generated steam condenses.

4. At the same time, when the pressure in the second bed becomes less than the evaporator pressure, the bed is opened to the heat exchanger HE1 and the vapor flows to the bed where it is adsorbed.

The previously described four steps represent the first half of the cycle. The second half of the cycle originates by circulating the heat transfer fluid in the reverse direction. During this second half of the cycle, bed I is cooled and adsorbs the formed vapor. Simultaneously, bed II is heated and generates the heating steam, which condenses inside the evaporator tubes.

Assumptions used in development of the model are:

- The adsorber pressure is uniform. Therefore, the vapor pressure and the adsorbent temperature are related by the adsorption equilibrium equation.
- The bed contents are in thermal equilibrium. Therefore, the adsorbent and the adsorbate have the same temperature.
- No heat losses to the surroundings.
- Model parameters, such as the fluid density, heat transfer coefficients, and velocity are assumed constant.

In above configuration the evaporator energy balance is identical to that of the TVC system, Eq. (3). The overall heat balance around the two adsorbers gives

$$M_m \lambda_m + M_d H''_{z1} = M_{cw} Cp \left(T_{cw_o} - T_{cw_i}\right) + M_d H''_s \tag{21}$$

where M_m, M_d, and M_{cw} are the mass flow rates of the motive steam, the formed vapor, and the utility cooling water, respectively; λ_m is the latent heat of the motive steam; H''_{z_1} and $H''s$ are the enthalpies of inlet and outlet water vapor; and T_{cw_o} and T_{cw_i} are the outlet and inlet temperatures of the utility water.

In the above equation, it is assumed that

- the mass of vapor adsorbed in the second bed is equal to the amount of steam generated in the first bed
- constant and equal rates for adsorption and desorption

- constant rate of heat exchange between the two beds.

Van Benthem et al. [25] proposed the use of an automatic bypass for the heat transfer fluid exchanging the heat between the two adsorbers. This resulted in keeping the heat flow rate at constant level within the system. Their experimental results showed that the use of the fluid bypass reduces the cooling capacity (adsorption speed) during the first part of the cooling process and increases it in the second part. Consequently, they obtained a nearly constant heat flow rate throughout the system. Also, they showed this arrangement improved the cycle thermal efficiency.

The purpose of water circulation is the cooling of the second bed from T_{e_2} to T_a, thus:

$$M_{cs}C_p\left(T_{cw_o}-T_{cw_i}\right)=M_zC_{p_z}\left(T_{e_2}-T_a\right) \quad (22)$$

On the other hand, the total heat removed from the second bed, Q_2, is expressed by the following equation

$$Q_2=M_d\lambda_v+M_zC_{p_z}\left(T_g-T_a\right)+M_dC_p\left(T_v-T_a\right) \quad (23)$$

A part of Q_2 is used to heat the first bed, Q_{21}, and the rest is rejected to the cooling water. Combining Eqs. (22) and (23) yields

$$Q_{21}=M_d\lambda_v+M_zC_{p_z}\left(T_g-T_{e_2}\right)M_dC_p\left(T_v-T_a\right) \quad (24)$$

The energy required to heat the first bed is given by

$$Q_1=M_d\lambda_s+M_zC_{p_z}\left(T_g-T_a\right)+M_dC_p\left(T_g-T_a\right) \quad (25)$$

This heat is supplied to the bed from two sources. The first part is the heat flow from the hot bed, Q_{21}, and the second part is gained from the motive steam. This balance is given by

$$Q_1=Q_{21}+M_m\lambda_m \quad (26)$$

Substituting Eqs. (24) and (25) in Eq. (26) gives

$$\begin{aligned}M_m\lambda_m&=M_zC_{p_z}\left(T_{e_2}-T_a\right)+M_dC_p\left(T_g-T_v\right)\\&=M_{cw}C_p\left(T_{cw_o}-T_{cw_i}\right)+M_dC_p\left(T_g-T_v\right)\end{aligned} \quad (27)$$

The function of the HE1 is identical the preheater unit used in the MVC system where the temperature of the intake seawater is increased from T_{cw} to T_f. This improves the thermal efficiency of the evaporator unit and the resulting plant performance ratio. The second heat exchange unit, HE2, is used to transfer heat from the desorption bed (bed II) to the cooling water stream. The thermal effectiveness of the HE2 is defined as

$$\eta=C_{p_z}\left(T_{e_2}-T_a\right)/\left[C_p\left(T_{e_2}-T_{cw_i}\right)\right] \quad (28)$$

However, the heat balance on the same heat exchanger is given by

$$M_zC_{p_z}\left(T_{e_2}-T_a\right)=M_{cw}C_p\left(T_{cw_o}-T_{cw_i}\right) \quad (29)$$

Combining Eqs. (28) and (29) gives

$$T_{e_2}=\left[T_{cw_o}-T_{cw_i}(1-\eta)\right]/\eta \quad (30)$$

For the heat transfer to take place between the second bed and the cooling water, the following relationships must be satisfied:

$$T_{cw_i}=T_a-\Delta T \quad (31)$$

$$T_{cw_o}=T_{e_2}-\Delta T \quad (32)$$

Van Benthem et al. [25] found that the optimum value of ΔT ranges between 3 and 5 °C.

The maximum and minimum temperatures of the two beds, T_g and T_a, are determined from the equilibrium relationship for the zeolite-water vapor system. This equilibrium is presented by the following equation, which was reported by Karagiorgas and Meunier [26]:

$$\ln(P) = a + b/T \tag{33}$$

where a and b are functions of the water content as follows:

$$a = 20.49 - 60.4\alpha + 787a^2 - 2.14 \times 10^3 \alpha^3 \tag{34}$$

$$b = -8013 + 33.83 \times 10^3 \alpha - 3 \times 10^5 \alpha^2 + 7.9 \times 10^5 \alpha^3 \tag{35}$$

where α is in kg of water per kg of zeolite, T is the temperature in °K, and P is the pressure in mbar. The adsorbent mass is obtained from the balance of water mass between states a and c.

$$M_z = M_m / (\alpha_g - \alpha_a) \tag{36}$$

Parameters in the model of the combined system include ΔT, η, α_a, T_s, T_g, and T_m. The following values were used in the solution of the model equations

$\Delta T = 5$ °C

$\eta = 0.9$

$\alpha_a = 0.06$ kg H_2O/kg zeolite

$T_g = (T_s + 8)$ °C

$T_m = (T_g + 8)$ °C

The calculations start with solution of Eq. (33) to determine T_a, which is obtained at a bed pressure equal to the vapor pressure of the vapor leaving the evaporator. This is followed by the solution of Eqs. (30)–(32) to determine T_{e_2}, T_{cw_i} and T_{cw_o}. The water content of the second bed, α_g, is obtained from Eq. (33) at the saturation pressure at T_g. The adsorbent mass is obtained from Eq. (36) and the flow rates of motive steam and utility water are determined from Eq. (27).

2.4. Absorption Vapor Compression (ABVC)

The absorption heat pumps are used on a large scale for airconditioning purposes. The ammonia-water heat pumps are used in these applications, with ammonia as the evaporating component. Other working fluids are pursued in the literature to meet industrial demand and applications other than airconditioning [23]. Working fluids, other than ammonia-water, include LiBr-water and hydroxide solutions, KOH and NaOH [27]. The absorption heat pumps include four main components, which include the generator, the absorber, the evaporator, and the condenser. The pump receives heat in the evaporator and the generator and rejects heat in the condenser and the absorber. The pump can be configured for simultaneous heating and cooling purposes.

A schematic for the proposed system is shown in Fig. 5. As is shown, the system contains six elements, which include the generator, the absorber, the evaporator/condenser, and three heat exchangers. In the proposed configuration, the evaporator desalination unit acts as the individual evaporator and condenser found in conventional absorption heat pumps. The process is described in the following points:

1. Saturated water vapor is generated at a flow rate of M_d in the evaporator. The vapor is routed to the absorber unit of the heat pump.
2. The absorption solution is LiBr, which is circulated between the absorber and the generator. The absorption process reduces the solution concentration and generates large

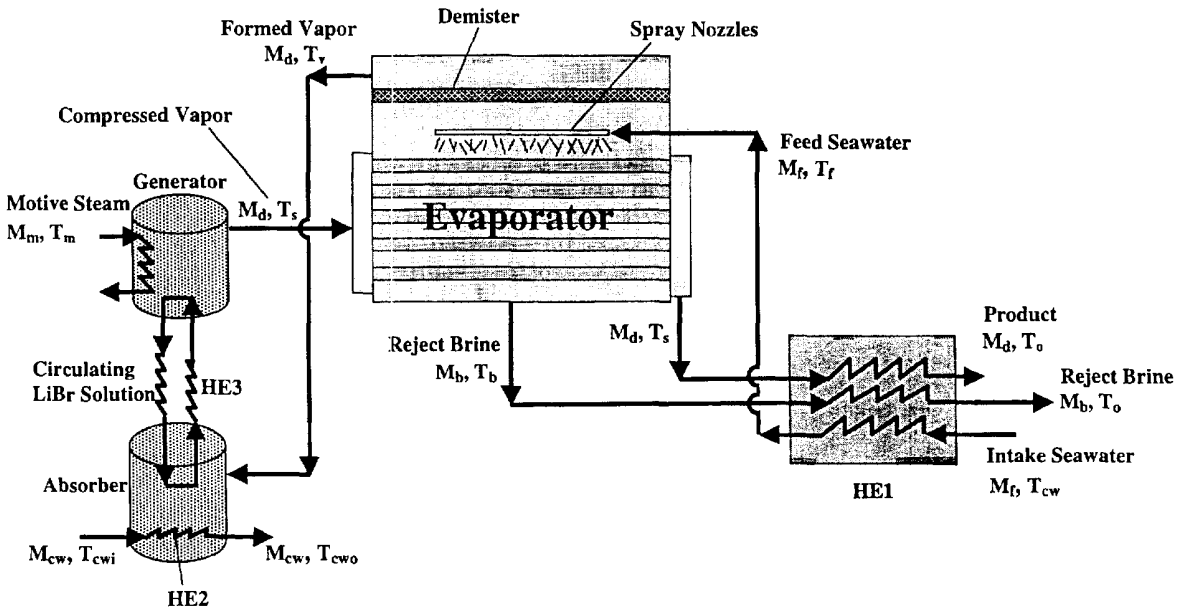

Fig. 5. A single-effect evaporator driven by an absorption heat pump.

amounts of heat. Part of this energy is used to generate hot utility water stream. The remaining part of the energy is transferred to the generator by the circulating LiBr solution.

3. The generator is used to concentrate the LiBr and to generate the steam necessary to drive the evaporator, M_d. The energy source for this process originates from the motive steam, M_m, and the circulating LiBr solution. The amount of steam of vapor formed in the generator is equal to the amount of vapor extracted from the evaporator.

4. The steam formed in the generator is used to drive the evaporator. The steam releases its latent heat, condenses, and is taken as the distillate product. The release of the latent heat results in the formation of the vapor in the evaporator.

5. The first heat exchanger is used to generate hot utility water, M_{cw}, by consuming part of the energy generated in the absorber unit.

6. The second heat exchanger is used to increase the temperature of the feed seawater, M_f, by exchanging heat with rejected brine, M_b, and the condensed distillate product, M_d.

7. The third exchanger transfers heat the LiBr solution leaving the generator to the LiBr solution flowing from the absorber to the generator.

The ABVC mathematical model includes balance equations for the elements of the heat pump. The balance equations include conservation of the system energy and the mass of LiBr. The balance of the seawater mass and its salt content are identical to Eqs. (1) and (2). The energy balance in the evaporator is identical to Eq. (3). Energy equations for the generator and absorber are then developed where the generator balance is

$$M_m \lambda_m = M_d H''_s + M_g Cp \left(T_{g_o} - T_{g_i}\right) \tag{37}$$

Also, the absorber energy balance, including the circulating LiBr heat exchanger, is

$$M_g Cp \left(T_{g_o} - T_{g_i}\right) + M_d H''_v = M_{cw} C_p \left(T_{cw_o} - T_{cw_i}\right) \tag{38}$$

The temperatures of the LiBr solution in the generator and absorber are assumed uniform and equal to the outlet stream temperature, T_{g_o} and T_{a_o}, respectively. The value of T_{g_o} is assumed in equilibrium with the temperature of the formed vapor, T_s. Similarly, the value of T_{a_o} is assumed in equilibrium with the temperature of the absorbed vapor, T_v. The saturation properties of the LiBr solution are calculated from the correlations given by Hellmann et al. [28]. The LiBr heat exchange unit (HE3) is analyzed in a similar manner to the heat exchange units of the ADVC system. This resulting equation is used to calculate the value of T_{g_i} where

$$T_{g_i} = T_{a_o} + \eta\left(T_{g_o} - T_{a_o}\right) \tag{39}$$

The addition of Eqs. (37) and (38) gives the overall energy balance on the generator and absorber, which is identical to that of the ADVC system, Eq. (21), or

$$M_m\lambda_m + M_d H''_v = M_d H''_s + M_{cw} C_p\left(T_{cw_o} - T_{cw_i}\right) \tag{40}$$

The overall mass balance on the generator gives

$$M_a = M_g + M_d \tag{41}$$

where M_a and M_g are the flow rates of the LiBr solution entering and leaving the generator, respectively. The balance of the LiBr mass is given by

$$M_a X_a = M_g X_g \tag{42}$$

The following specifications are made in order to solve the above system of equations:

- The temperatures of the motive steam, T_m, and the steam formed in the generator, T_s
- The flow rate of the LiBr solution, M_a, is set equal to 14 times M_d
- The mass fraction of LiBr in stream, X_g, is set equal to 0.65
- The temperature of the cooling water stream, T_{cw_o} and T_{cw_i}, are set equal to 90 and 25°C, respectively.

The solution of the above system starts with calculations of the saturation temperatures of the LiBr solution, T_{g_o} and T_{a_o}, which are determined at T_s and T_v. The temperature of the LiBr solution entering the generator, T_{g_i}, is calculated from Eq. (39). The flow rate and concentration of the LiBr streams are obtained from Eqs. (41) and (42). The flow rate of utility water is calculated from Eq. (38). Finally, the motive steam flow rate is determined from Eq. 40.

3. Results and discussion

The performance of the four single systems is described in terms of

- the performance ratio, $PR = M_d/M_m$
- the specific heat transfer area, $sA = (A_e+A_c)/M_d$
- the specific cooling water flow rate, $sM_{cw} = M_{cw}/M_d$
- the specific consumption power for the MVC system, W.

The performance of the MVC, ABVC, and ADVC are analyzed in terms of the top brine temperature and the temperature difference of the boiling brine and compressed vapor. On the other hand, the performance of the TVC system is determined in terms of the brine boiling temperature and the pressure of motive steam.

The following values are used to define the system parameters:

- the brine boiling temperature range is 40 to 110°C

- the pressure range of motive steam in the TVC system is 250–1500 kPa
- the compression ratio is 2.
- the temperature range of compressed vapor in MVC, ABVC, and ADVC is higher than the brine boiling temperature by 2–12°C
- the flow rate of product distillate is 1 kg/s
- the temperature of intake seawater is 25°C
- the influent temperature of cooling water in the ABVC system is 25°C
- the salinity of feed and reject brine are set at 42,000 and 70,000 ppm, respectively.

The specific power consumption of the MVC system and the performance ratio of the other systems are shown in Figs. 6–9. The specific power consumption of the MVC system (Fig. 6) varies over a range of 7–19 kWh/m^3 as a function of the boiling temperature and the temperature difference of the compressed vapor and the boiling brine. The specific power consumption increases at larger temperature differences. This result is expected because of the higher energy demand required to increase the temperature of the compressed steam over a larger range. The decrease in the specific power consumption at higher boiling temperatures is caused by the decrease in specific volume of inlet vapor at higher temperatures. The predicted model results for the power consumption are consistent with values reported in industrial practice, which ranges between 6–16 kWh/m^3. It should be noted that the predicted specific power consumption depends strongly on the used value for the compressor efficiency.

The performance ratio of the TVC system is shown in Fig. 7. As is shown, higher performance is obtained at low brine temperatures and high motive steam pressures. The decrease in the system performance at high temperatures is caused by the increase in motive steam consumption. This is caused by increase of the vapor pressure at higher temperatures. Therefore, larger amounts of motive steam are needed to compress the vapor to higher pressures. Use of high-pressure motive steam improves the system performance ratio. The high-pressure motive steam posses sufficient energy to compress large amounts of the entrained vapor. For example, at motive steam pressures of 1,000–1,500 kPa and a boiling temperature of 40°C, the system performance ratio is close to 2. This value drops by 25% at lower motive steam pressures, i.e., 250 kPa.

Performance ratio results for the ADVC and ABVC are shown in Figs. 8 and 9. Variations in the system performance ratio show similar behavior to those of the TVC and MVC systems. The performance ratio decreases at higher boiling temperatures and higher temperature differences between the boiling brine and the compressed vapor. The same argument given for the TVC system applies for both systems, where at higher temperatures and pressure, larger amounts of the motive steam are required to compress the entrained vapor. Both systems show higher potential for reaching performance ratios exceeding those of the TVC and the MVC systems. As is shown in Figs. 8 and 9, the performance ratio for both systems varies between 4 and 5 at low steam temperatures. Moreover, at higher steam temperatures the system performance remains at high values above 3. This behavior is due to proper management of energy within the system. In the ABVC system, the motive steam is used to provide sensible heat to the adsorbed water and the solid bed. On the other hand, the fluid circulating between the two beds provides the major portion of the energy consumed by the compressed vapor. The circulating fluid transfers the exothermic energy generated from the adsorption bed to the desorption bed. The same concept applies for the ABVC system where the motive steam is used to provide sensible heat to LiBr-water solution in the generator. The circulating LiBr-water solution transfers part of the exothermic heat generated during absorption to the generator. This provides the energy required for generation of the compressed vapor.

The heat transfer area for the above systems

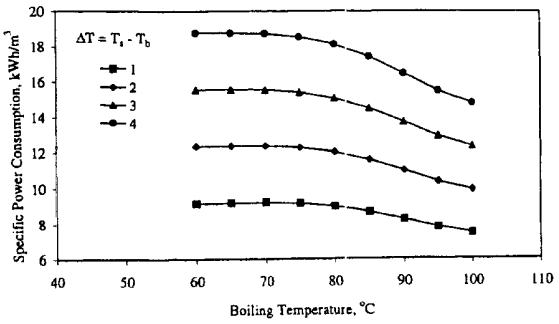

Fig. 6. Variation in specific power consumption in MVC as a function of boiling temperature and temperature difference of condensing steam and boiling brine.

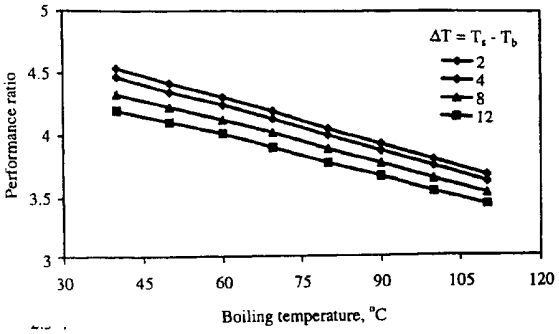

Fig. 8. Effect of boiling temperature and the temperature difference of compressed vapor and boiling brine on the performance ratio of the ADVC system.

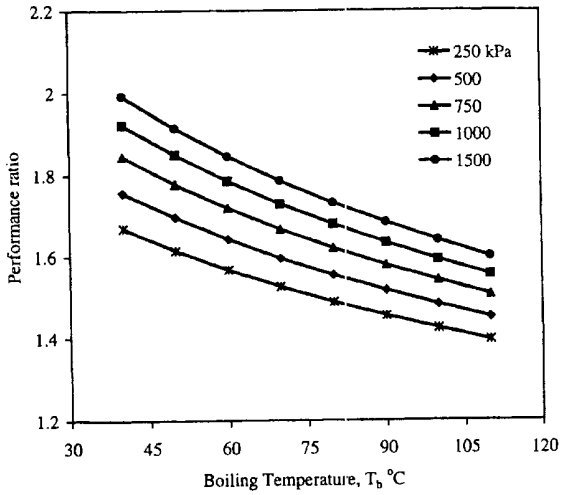

Fig. 7. Effect of boiling temperature and the motive steam pressure on performance ratio of the TVC system.

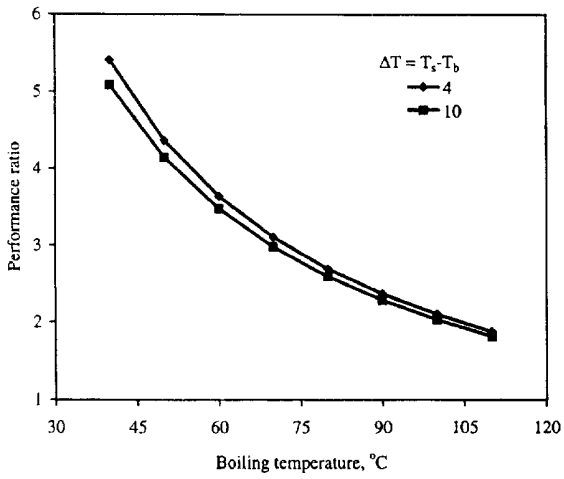

Fig. 9. Effect of boiling temperature and the temperature difference of compressed vapor and boiling brine on the performance ratio of the ABVC system.

include the following:

- the evaporator in all systems
- the down condenser area in the TVC system
- the feed preheater areas in the MVC, ABVC, and ADVC systems
- the cooling water heat exchanger in the ABVC and ADVC systems.

The evaporator area in the TVC system differs from those found in the other three systems. This is because the amount of compressed vapor in the MVC, ABVC, and ADVC is equal to the amount of vapor formed in the evaporator. The amount of compressed vapor in the TVC system is equal to the sum of the entrained vapor and the motive steam. This total amount is larger than the amount of vapor formed in the evaporator, which is necessary to balance the evaporator energy.

Fig. 10 illustrates variations in the evaporator specific surface area for the MVC, ABVC, and ADVC systems. The evaporator specific heat transfer area in the TVC system is shown in

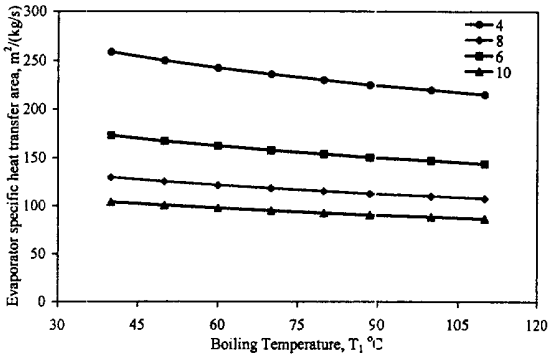

Fig. 10. Effect of boiling temperature and the temperature difference of compressed vapor and boiling brine on the evaporator-specific heat transfer area for the MVC, ADVC, and ABVC systems.

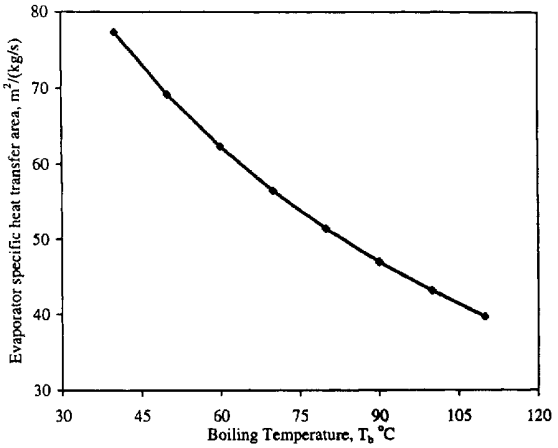

Fig. 11. Effect of boiling temperature on the specific surface area of the evaporator for the TVC system.

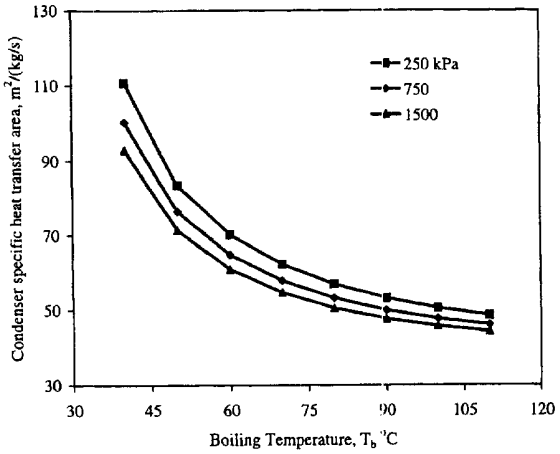

Fig. 12. Effect of boiling temperature and the motive steam on the specific surface area of the condenser for the TVC system.

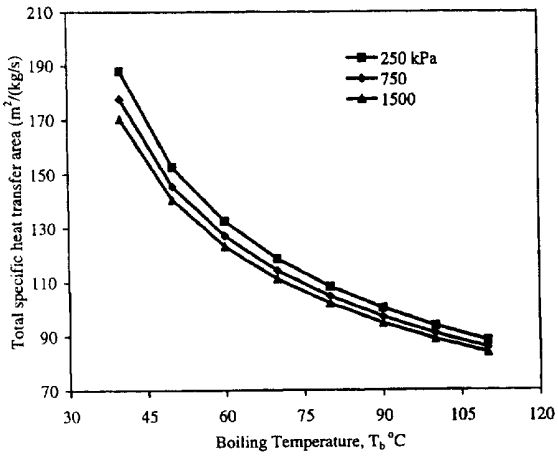

Fig. 13. Effect of boiling temperature and the motive steam pressure on the total specific heat transfer area for the TVC system.

Fig. 11. The specific heat transfer area decreases drastically at high boiling temperatures. This result is previously presented by El-Dessouky et al. [14] in the analysis of the MEE system, El-Dessouky [2] in the analysis of TVC system, and by El-Dessouky and Ettouney [3] in the analysis of the hybrid systems of MEE and heat pumps. The overall heat transfer coefficient increases at higher boiling temperatures. This enhances the heat transfer rates and in turn reduces the heat transfer area. As is shown in both figures, the specific heat-transfer area decreases at higher boiling temperatures. Results for the specific heat-transfer area in the down condenser and total specific heat transfer area in the TVC system are shown in Figs. 12 and 13. The behavior and results shown in both figures are similar to those obtained for the evaporator.

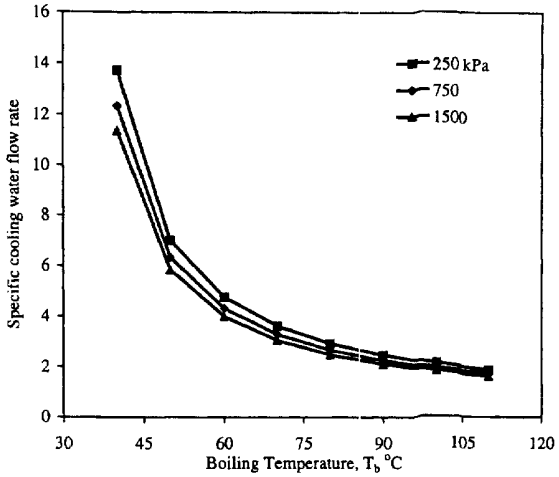

Fig. 14. Effect of boiling temperature and the motive steam pressure on the specific cooling water flow rate for the TVC system.

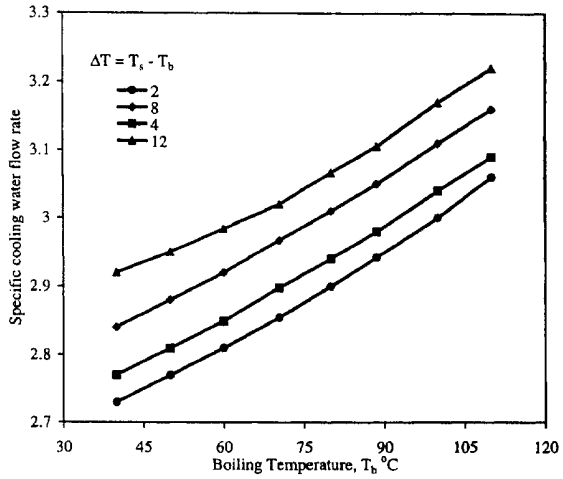

Fig. 15. Effect of boiling temperature and the temperature difference of compressed vapor and boiing brine for the ADVC.

Use of cooling water is found in the TVC, ADVC, and ABVC system. The cooling water removes excess energy added to the system by the motive steam. The MVC system does not require the use of any cooling water because the entire formed vapor is compressed and then condensed inside the evaporator tubes. The effluent temperature of the cooling water in the TVC system is 35°C. This differs considerably from the effluent temperature of the utility cooling water in the ABVC and the ADVC systems, which may reach a high value close to 90°C. The results for the specific cooling flow rate are shown in Figs. 14 and 15 for the TVC and the ADVC systems, respectively. The results for the TVC system show decrease in the specific cooling water flow rate upon the increase of the motive stream pressure and the brine boiling temperature. At higher motive steam pressures the amount of entrained vapor is increased. This reduces the amount of vapor routed to the condenser, which in turn reduces the condenser specific heat transfer area and the specific cooling water flow rates. At higher boiling temperatures, the heat-transfer coefficient increases, which improves the rate of heat transfer across the condenser tubes. In turn, this reduces the specific heat transfer area as well as the specific water cooling flow rate. The cooling water in the ABVC and the ADVC systems is used to remove excess heat in the absorber and adsorber, respectively. The amount of heat generated increases at higher boiling temperatures.

4. Conclusions

In summary, the following conclusions are made:

- Predictions of all models show very good agreement with available industrial data and known practice, i.e., performance ratio, specific power consumption, specific heat transfer area, and specific cooling water flow rate.
- The performance ratio for the four single-effect vapor compression systems has values higher than one.
- The performance ratio for the four systems increases at low boiling temperatures.
- The specific power consumption increases in the MVC system at higher temperature difference of compressed steam and boiling brine.

- The performance ratio of the TVC system increases at higher motive steam pressures.
- The performance ratio in the ABVC and the ADVC systems is higher at low temperature difference of the compressed vapor and boiling temperature.
- The MVC system requires no cooling water; however, use of a feed preheater is necessary to increase the temperature of the feed seawater. This is made by recuperation of the thermal energy in the reject brine and condensed vapor.
- The TVC, ABVC, and ADVC require cooling water to remove excess heat in the system provided by the motive steam.
- The ABVC and ADVC systems generate hot utility water, which can be used in other applications.
- The ABVC and ADVC have great potential in the desalination industry because of their higher performance ratio and better energy management.
- The specific heat transfer area in the evaporator, condenser, and preheater is drastically reduced at higher boiling temperatures.
- The specific cooling water flow rate in the TVC system is lower at higher boiling temperatures and motive steam pressures.
- The specific cooling water flow rate increases in the ABVC and ADVC systems at higher boiling temperatures and upon the increase of the temperature difference of the compressed vapor and the boiling brine.

5. Symbols

A — Heat transfer area, m^2
BPE — Boiling point elevation, °C
C_p — Heat capacity, kJ/kg °C
Cr — Compression ratio
H — Enthalpy of liquid water, kJ/kg
H'' — Enthalpy of water vapor, kJ/kg
$LMTD$ — Logarithmic mean temperature difference, °C
M — Mass flow rate, kg/s
M_z — Mass of adsorbing solids, kg
P — Pressure, kPa
PCF — Pressure correction factor
PR — Performance ratio
Q — Heat transfer rate, kJ/s
Ra — Entrainment ratio
sA — Specific heat transfer area, $m^2/(kg/s)$
$sMcw$ — Specific cooling water flow rate
ΔT — Temperature drop, °C
T — Temperature, °C
TCF — Temperature correction factor
U — Overall heat transfer coefficient, kW/m^2 °C
V — Vapor specific volume, m^3/kg
W — Specific power consumption, kJ/m^3
X — Salt mass fraction

Greek

α — Adsorption capacity, kg water/kg zeolite
γ — Isentropic index
η — Efficiency
λ — Latent heat, kJ/kg

Subscripts

a — Adsorption bed or absorber
b — Brine
c — Condenser or condensate
cw — Cooling water
d — Distillate vapor
e — Evaporator
ev — Entrained vapor or adsorbed water
f — Feed seawater
g — Desorption bed or generator
h — Difference of formed and entrained vapor
i — Inlet stream
m — Motive steam
o — Outlet stream
s — Compressed vapor
v — Formed vapor

References

[1] IDA Worldwide Desalting Plants Inventory, Wangnick, Report No. 13, International Desalination Association, Gnarrenburg, 1995.
[2] H. El-Dessouky, Modeling and simulation of thermal vapor compression desalination plant, Symposium on Desalination of Seawater with Nuclear Energy, Taejon, Republic of Korea, 1997.
[3] H.T. El-Dessouky and H.M. Ettouney, Hybrid multiple effect evaporation/heat pump water desalination systems, IDA Seminar, Cairo, Egypt, 1997.
[4] N.M. Wade, Desalination, 93 (1993) 343.
[5] O.J. Morin, Desalination, 93 (1993) 69.
[6] G. Hess and O.J. Morin, Desalination, 87 (1992) 55.
[7] M.A. Darwish and H. El-Dessouky, Applied Thermal Engineering, 18 (1996) 523.
[8] R. Rautenbach, Desalination, 93 (1993) 1.
[9] R. Rautenbach, J. Widua and S. Schafer, Proc., IDA World Congress on Desalination and Water Sciences, Abu Dhabi, 1 (1995) 117.
[10] H.T. El-Dessouky and G.R. Assassa, Desalination, 55 (1985) 145.
[11] M.A. Darwish and A.A. El-Hadik, Desalination, 60 (1986) 251.
[12] W.T. Hanbury, Proc., IDA World Conference on Desalination and Water Science, Abu Dhabi, UAE, 4 (1995) 375.
[13] K. Minnich, J. Tonner and D. Neu, Proc., IDA World Congress on Desalination and Water Science, Proc. Int. Symp. Abu Dhabi, 3 (1995) 233.
[14] H.T. El-Dessouky, I.M. Alatiqi and S. Bingulac, Proc., IDA World Congress on Desalination and Water Sciences, Madrid, Spain, 1 (1997) 119.
[15] C. Temstet and J. Laborie, Proc., IDA World Congress on Desalination and Water Science, Proc. Int. Symp. Abu Dhabi, 3 (1995) 297.
[16] C. Temstet, G. Canton, J. Laborie and A. Durante, Desalination, 105 (1996) 109.
[17] Z. Zimerman, Desalination, 96 (1994) 51.
[18] M.A. Darwish and H. El-Dessouky, Proc., IDA World Congress on Desalination and Water Sciences, Abu Dhabi, 2 (1995) 219.
[19] J.M. Veza, Desalination, 101 (1995) 1.
[20] M. Lucas and B. Tabourier, Desalination, 52 (1985) 123.
[21] R. Matz and Z. Zimerman, Desalination, 52 (1985) 201.
[22] T. Michels, Desalination, 93 (1993) 111.
[23] G. Alefeld and F. Ziegler, ASHRAE Tech. Data Bull., June 1985, pp. 11–24.
[24] K. Fathalah and S.E. Aly, Energy Convers., 31 (1991) 529.
[25] G.H.W. Van Benthem, G. Cacciola and G. Restuccia, Heat Recovery Systems & CHP, 15 (1995) 531.
[26] M. Karagiorgas and F. Meunier, Heat Recovery Systems & CHP, 7 (1987) 285.
[27] A.S. Beutler, G.R. Feuerecker and G. Alefeld, ASHRAE Trans.: Symposia, AT-96-17-4, 1996.
[28] H.M. Hellmann and G. Grossman, ASHRAE Trans. Sym., 1996, pp. 980–997.

Appendix A: Thermodynamic properties of saturated water

The following correlations are used to calculate the thermodynamic properties of saturated water. The correlations include:

- the saturation temperature

$$T = 41.976635 + 0.735578P - 2.182991\times10^{-3}P^2 + 3.374442\times10^{-6}P^3 - 2.650837\times10^{-9}P^4 + 1.013988\times10^{-12}P^5 - 1.498537\times10^{-9}P^6 \quad \text{(A1)}$$

with a range of 4–2104 kPa and $R^2 = 0.9915$.

- the saturation pressure

$$P = 10.1724607 - 0.6167302T + 1.832849\times10^{-2}T^2 - 1.77376\times10^{-4}T^3 + 1.47068\times10^{-6}T^4 \quad \text{(A2)}$$

with a range of 30–215 °C and $R^2 = 0.9999$.

- The specific vapor volume

$$v = 163.3453 - 8.04142177T + 0.17102116T^2 - 1.878124\times10^{-3}T^3 + 1.03842\times10^{-5}T^4 - 2.28215\times10^{-8}T^5 \quad \text{(A3)}$$

with a range of 20–130 °C and R^2=0.9998.

- The vapor enthalpy

$$H'' = 2500.152 + 1.947036T - 1.945387\times10^{-3}T^2 \quad \text{(A4)}$$

with a range of 0.01–145 °C and $R^2 = 0.9999$.

- The liquid enthalpy

$$H = 0.5802129 + 4.151904T + 3.536659\times10^{-4}T^2 \quad \text{(A5)}$$

with a range of 0.01–145 °C and $R^2 = 0.9999$.